

UNCLASSIFIED

AD NUMBER
AD234625
NEW LIMITATION CHANGE
TO Approved for public release, distribution unlimited
FROM Distribution authorized to U.S. Gov't. agencies and their contractors; Administrative/Operational Use; Jun 1959. Other requests shall be referred to Wright Air Development Center, Materials Lab., Wright-Patterson AFB, OH 45433.
AUTHORITY
AFAL ltr dtd 17 Aug 1979

THIS PAGE IS UNCLASSIFIED

UNCLASSIFIED

AD 234625

DEFENSE DOCUMENTATION CENTER

FOR

SCIENTIFIC AND TECHNICAL INFORMATION

CAMERON STATION, ALEXANDRIA, VIRGINIA



UNCLASSIFIED

CATALOGED BY WWAD

TI. 57.746

WADC TECHNICAL REPORT 53-192
PART XIV

DO NOT DESTROY
RETURN TO
WWAD—LIBRARY

FILE COPY

MECHANISM OF RAIN EROSION

Part XIV. Pits in Metals Caused by Collusion with Liquid
Drops and Rigid Steel Spheres

Clive G. Engel

National Bureau of Standards

MAY 1960

This report is not to be announced or distributed automatically
to foreign governments (AFR 205-43A, paragraph 6d).

WRIGHT AIR DEVELOPMENT DIVISION

NOTICES

When Government drawings, specifications, or other data are used for any purpose other than in connection with a definitely related Government procurement operation, the United States Government thereby incurs no responsibility nor any obligation whatsoever; and the fact that the Government may have formulated, furnished, or in any way supplied the said drawings, specifications, or other data, is not to be regarded by implication or otherwise as in any manner licensing the holder or any other person or corporation, or conveying any rights or permission to manufacture, use, or sell any patented invention that may in any way be related thereto.

- - - - -

Qualified requesters may obtain copies of this report from the Armed Services Technical Information Agency, (ASTIA), Arlington Hall Station, Arlington 12, Virginia.

- - - - -

Copies of WADC Technical Reports and Technical Notes should not be returned to the Wright Air Development Center unless return is required by security considerations, contractual obligations, or notice on a specific document.

WADC TECHNICAL REPORT 53-192

PART XIV

MECHANISM OF RAIN EROSION

Part XIV. Pits in Metals Caused by Collision with Liquid
Drops and Rigid Steel Spheres

Olive G. Engel

National Bureau of Standards

MAY 1960

Materials Central

Contract No. AF 33 (616) -59-3

Project No. 7340

WRIGHT AIR DEVELOPMENT DIVISION
AIR RESEARCH AND DEVELOPMENT COMMAND
UNITED STATES AIR FORCE
WRIGHT-PATTERSON AIR FORCE BASE, OHIO

FOREWORD

This report was prepared by the National Bureau of Standards under USAF Contract No. AF(616)-59-3. The contract was initiated under Project No. 7340, "Nonmetallic and Composite Materials", Task No. 73400, "Organic and Inorganic Plastics". The project was administered under the direction of the Materials Central, Directorate of Advanced Systems Technology, Wright Air Development Division, with Mr. George P. Peterson acting as project engineer.

The experimental work that is reported was accomplished with the co-operation of Convair, Division of General Dynamics Corporation, and of the U. S. Naval Research Laboratory.

This report covers the period of work from about October 1957 to June 1959.

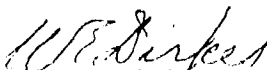
ABSTRACT

A pit-depth-versus-velocity equation developed earlier for high-speed collision of liquid drops and soft, ductile metal spheres against targets of the soft and medium-hard metals was tested further with experimental data obtained using target plates of electrolytic tough pitch copper, 1100-0 aluminum, and 2024-0 aluminum, the static strength properties of which were measured by testing tensile specimens. The projectiles used to produce the pits were mercury drops, waterdrops, and steel spheres. It was found that the numerical constants in the equation are different for projectiles that flow during and as a result of the collision than for projectiles that do not flow (hardened steel spheres). Curves calculated by the equation were found to be in acceptable agreement with experimental pit-depth-versus-velocity data for collisions of the indicated projectiles with target plates of the three metals used, with the exception of the case of steel-sphere impingement against 2024-0 aluminum alloy. In this case work-hardening of the target metal seems to foster a mode of pit formation that was not considered in the development of the pit-depth-versus-velocity equation.

PUBLICATION REVIEW

This report has been reviewed and is approved.

FOR THE COMMANDER:



W. E. Dirkes
Chief, Plastics Branch
Nonmetallic Materials Laboratory
Materials Central

TABLE OF CONTENTS

Section	Page
1. Introduction	1
1.1 Preparation of Target Plates	3
1.2 Determination of Static Tensile Properties of the Metals Used	4
2. Liquid-versus-Solid Collisions	5
2.1 Collisions between Metal Target Plates and Mercury Drops	8
2.2 Collisions between Metal Target Plates and Waterdrops	14
3. Solid-versus-Solid Collisions	18
3.1 Collisions of Steel Spheres with Target Plates of 1100-0 Aluminum	19
3.2 Collisions of Steel Spheres with Target Plates of Annealed Electrolytic Tough Pitch Copper	21
3.3 Collisions of Steel Spheres with Target Plates of 2024-0 Aluminum	25
3.4 Collisions of Steel Spheres with Target Plates of 2024-0 Aluminum that Were Backed with a Heavy Steel Supporting Block	35
4. Liquid-versus-Liquid Collisions	38
REFERENCES	41

LIST OF ILLUSTRATIONS

Figure	Page
1 Collisions of Mercury Drops of Two Sizes against Annealed Electrolytic Tough Pitch Copper . . .	10
2 Collisions of Mercury Drops of Two Sizes against 2024-O Aluminum	13
3 Collisions of 0.2-cm Waterdrops against Annealed Electrolytic Tough Pitch Copper	15
4 Collisions of 0.2-cm Waterdrops against 2024-O Aluminum	17
5 Collisions of Steel Spheres of Three Sizes against 1100-O Aluminum	22
6 Collisions of Steel Spheres of Three Sizes against Annealed Electrolytic Tough Pitch Copper	24
7 Collisions of Steel Spheres of Three Sizes against 2024-O Aluminum	27
8 Cross Sections of Pits Produced by Collisions of a 1/2-in. Steel Sphere with Annealed Electrolytic Tough Pitch Copper and with 2024-O Aluminum	29
9 Shear Stresses Produced in a Metal Plate by an Impinging Steel Sphere	32
10 Stress-Strain Curves for 1100-O Aluminum, 2024-O Aluminum, and Annealed Electrolytic Tough Pitch Copper	34
11 Best-Fit Curves for Collisions of Steel Spheres against 2024-O Aluminum Targets that Were Backed with a Heavy Steel Supporting Block . .	37
12 Schematic Representation of Projectile-Target Collision Types	40

LIST OF TABLES

<u>Table</u>	<u>Page</u>
1. Static Tensile Properties of the Metals Used , . .	5
2. Constants of the Material of Projectile and Target	7
3. Experimental Data for Collisions of Mercury Drops with Annealed Electrolytic Tough Pitch Copper .	9
4. Experimental Data for Collisions of Mercury Drops with 2024-0 Aluminum	12
5. Experimental Data for Collisions of Waterdrops with Annealed Electrolytic Tough Pitch Copper .	16
6. Experimental Data for Collisions of Waterdrops with 2024-0 Aluminum	16
7. Experimental Data for Collisions of Steel Spheres with 1100-0 Aluminum	20
8. Experimental Data for Collisions of Steel Spheres with Annealed Electrolytic Tough Pitch Copper .	23
9. Experimental Data for Collisions of Steel Spheres with 2024-0 Aluminum	26
10. Experimental Data for Collisions of 5/16-in. Steel Spheres with a 2024-0 Aluminum and 1100-0 Aluminum Combination Target	31
11. Experimental Data for Collisions of Steel Spheres with 2024-0 Aluminum Backed with a Steel Sup- porting Block	36

1. Introduction

Collisions between liquids and solids in all of the possible projectile-target combinations in which they can occur have been topics for research. Some of these are: solid-versus-solid collisions (artillery experiments), solid-versus-liquid collisions (water-entry problems), liquid-versus-solid collisions (high-speed rain-erosion research), and liquid-versus-liquid collisions (impact of solids at meteor velocities). Work has been done at the National Bureau of Standards toward developing an equation that will give pit depth as a function of impingement velocity for collisions of target plates of the soft and medium hard metals with drops of liquids [1].^a

The model on which the equation is based is the movement of the core of metal of the target plate immediately under the collision area with respect to the remainder of the plate. In order that the core of metal through the target plate under the collision area may be free to move, the side of the plate opposite to that on which the collision occurs must be a free surface. In addition to this condition on the target plate, it must not be so thin that it bends as a whole under the collision, or so thick that the spread of the compressional wave that passes through it as a result of the collision is appreciable.

^a Numbers in brackets refer to literature references at the end of this report.

Manuscript released by the author June 1959 for publication as a WADC Technical Report.

In the development of this pit-depth-versus-velocity equation, such characteristic fluid-flow parameters as the Weber Number and the Reynolds Number were neglected. The equation should, therefore, apply equally well to pits caused by collisions of solid spheres with target plates of the soft and medium hard metals.

In the case of collisions of solid-sphere projectiles that flow like a liquid drop during and as a result of the collision, the equation should apply without modification even of the numerical constants. It has, indeed, been found that the equation does produce curves that fit pit-depth-versus-velocity data for high-speed collisions of soft ductile metal spheres against targets of the same metals [1].

For the case of collisions of hardened steel spheres, the numerical constants in the equation will be different. These spheres do not flow during the collision; none of the collision energy is lost in the flow of the projectile and, therefore, a larger amount of it is used in forming the pit.

Pit-depth-versus-velocity data^b for high-speed collisions of liquid drops with metal plates were used to evaluate the numerical constants in the equation and to test the equation. These data were of a preliminary nature. The yield strengths of the metals that were used for the target plates were not determined by experiment.

It is important to know the static yield strength of the target metal. Although it is the dynamic yield strength that must be used in the equation, the dynamic yield strength may be expected to vary in the same direction that the static yield strength varies for different heat-treatment states of a given metal. Different sets of pit-depth-

These data were obtained at Convair, Division of General Dynamics Corporation, in San Diego, California. See Reference [1].

versus-velocity data will not, in general, be comparable unless the static yield strength of the metal target plates that are used is essentially the same. Furthermore, the static yield strength can be used to calculate the dynamic yield strength in the case of the Duralumins [2] and closely related aluminum alloys.

The work described in this report is an effort to test the equation further by determining the depth of pits that are produced by waterdrops, mercury drops, and steel spheres on collision with target plates of 1100-0 aluminum, 2024-0 aluminum, and annealed electrolytic tough pitch copper the static yield strengths of which were determined by experiment.

1.1 Preparation of the Target Plates

Plates of the metals to be used were obtained in 1-in. thickness so that 6-x-6-in. target plates cut from them would be approximately 2 to 4.5 sphere diameters thick for use in experiments involving impingement of 7/32-in.-, 5/16-in.-, and 1/2-in.- diameter steel spheres. Tensile specimens for determining the static yield strength and small 1/8-in.-thick target plates for use in experiments involving collision with 0.1-cm and 0.2-cm mercury drops and waterdrops were machined from some of this material.

The 1100-0 aluminum was obtained from the Davenport Works of the Aluminum Company of America in Riverdale, Iowa. The material was furnished in mill finish and was as scratch-free as was commercially feasible. For the annealing process the objects were placed in the furnace while it was cold. The furnace temperature was then brought up to 650°F and was held at 650°F for 4.5 hours in the case of the large target plates and the tensile specimens and for about 2 hours in the case of the small target plates. The furnace was then turned off and the objects were allowed to cool with the furnace. The tensile specimens were suspended in the vertical position during the annealing process to prevent sagging.

The 2024-0 aluminum was obtained as 2024-T4 aluminum at the U. S. Naval Research Laboratory in Washington, D.C.

The tensile specimens and the target plates of this metal were put into the furnace after it had been raised to a temperature of 750°F and they were heated at 750°F for 4 hours. They were cooled to 350°F at a rate of 46°F per hour and were then removed from the furnace.

The electrolytic tough pitch copper was obtained from the American Brass Company. For annealing the objects were placed in the furnace after it had attained a temperature of 800°F. The large target plates were kept in the hot furnace for approximately one hour, the small target plates for about 40 min, and the tensile specimens for about 30 min. The objects were in each case removed from the furnace at the end of the specified time and were air cooled. The copper oxide that formed was removed from the target plates by pickling in dilute acid and by gentle abrasion.

1.2 Determination of Static Tensile Properties of the Metals Used

The tensile specimens were standard ASTM test specimens having 0.505-in. diameter in accordance with ASTM designation E 8-54 T. They were tested in a standard testing machine in NBS Engineering Mechanics Section using autographic recording equipment. The data obtained were yield strength (0.2 percent offset), tensile strength, and elongation in 2 inches. The test results are given in Table 1.

Table 1 Static Tensile Properties of the Metals Used			
Metal	Yield Strength psi	Tensile Strength psi	Elongation percent
1100-0 Aluminum	2,650	11,350	41.0
1100-0 Aluminum	2,600	11,100	41.5
2024-0 Aluminum	12,600	28,400	17.5
2024-0 Aluminum	12,700	29,000	17.5
2024-0 Aluminum	12,600	30,000	18.0
2024-0 Aluminum	12,600	30,300	18.5
Annealed Copper	4,200	30,800	50.0
Annealed Copper	4,300	31,000	49.0
Annealed Copper	3,700	31,200	54.0
Annealed Copper	3,700	31,100	53.0

2. Liquid-Versus-Solid Collisions

The small target plates of 1100-0 aluminum, 2024-0 aluminum, and annealed electrolytic tough pitch copper that were prepared were sent to Convair, Division of General Dynamics Corporation, in San Diego, California, to be fired into drops of mercury (0.1 cm and 0.2 cm in diameter) and drops of water (0.2 cm in diameter) at high speed. When the tests were made, the 1100-0 aluminum target plates were not fired because they were too thin.

The mercury drops used in the firings were individually weighed on an analytical balance. The actual diameters of the mercury drops and waterdrops varied in most cases by less than ± 10 percent of the indicated size. The depths of the pits that were produced were measured at Convair with use of an optical micrometer; the depth measurements were reported

to be good to +0.0005 inch.

The theoretical curves for the liquid-drop-versus-solid-target collisions were obtained with use of the equations [1]

$$\delta_1 = \frac{7.2 d z}{c (x + z')} \left[V - V_1 \right] \quad (1)$$

and

$$V_1 = \frac{19 E' (z + z')}{(\rho c' z'^3)^{1/2}} \quad (2)$$

in which δ_1 is pit depth, d is drop diameter, c is the speed of sound in infinite medium, ρ is the density, z is the acoustic impedance ($z = c \rho$), E' is the dynamic compressive yield strength of the target metal, V_1 is the smallest impingement velocity at which a permanent pit is made and V is the impingement velocity. Primed quantities refer to the material of the target plate and unprimed quantities refer to the material of the liquid drop. All quantities are in cgs units. Values of these quantities for the materials used for projectiles and targets are listed in Table 2.

The development of Eqs (1) and (2) has been given previously [1]. The conditions for valid use of these equations were discussed in Section 1.

Table 2
Constants of the Material of Projectile and Target

Constant	Projectile				Target	
	Water	Mercury	Steel	1100-O Aluminum	2024-T0 Aluminum	Copper, Electrolytic
Sound Speed, c cm/sec	$1.497 \times 10^5^c$	$1.451 \times 10^5^c$	$5.786 \times 10^5^d$	$6.318 \times 10^5^d$	$6.370 \times 10^5^d$	$4.691 \times 10^5^d$
Density, ρ g/cm ³	0.99707^e	13.546^e	7.859^f	2.713^g	2.768^g	8.92^e
Acoustic Impedance, h g/(cm ² sec)	0.1493×10^6	1.966×10^6	4.547×10^6	1.714×10^6	1.763×10^6	4.184×10^6
Dynamic Yield Strength, Y' dynes/cm ²	-----	-----	-----	$7.239 \times 10^8^i$	$2.350 \times 10^9^i$	$2.394 \times 10^9^j$

c Data from Bergmann [3].

d Values measured by Mr. C. E. Tschiesse of NBS Sound Section.

e Handbook of Chemistry and Physics.

f Metals Handbook.

g Aluminum Company of America.

h Acoustic Impedance is the product of sound speed and density, $z = c\rho$.

i Dynamic yield strengths of the aluminum alloys were calculated from estimates given by Whiffin [4] for the ratio of the dynamic to the static yield strength.

j Dynamic yield strength of copper is that given by Whiffin [2].

2.1 Collisions between Metal Target Plates and Mercury Drops

The experimental pit depths for collisions of 0.1- and 0.2-cm mercury drops against target plates of annealed electrolytic tough pitch copper are listed in Table 3. They are plotted in Figure 1 along with theoretical curves that were calculated with use of Eqs (1) and (2) and the data of Table 2.

It can be seen from Figure 1 that the theoretical curves are in relatively good agreement with the experimental points. The effect of the change in drop size is properly accounted for by the theoretical equations. Curve A, calculated for the 0.1-cm drop size, is in better agreement with the observed depths produced by collision with 0.1-cm drops than Curve B, calculated for the 0.2-cm drop size, is with the observed depths produced by collision with 0.2-cm drops. Drop diameters calculated from the weight of the mercury drops can be expected to be more accurate for the smaller drop size. In this connection, it is noteworthy that there is more scatter in the experimental data for the 0.2-cm drop size.

On the other hand, if the calculated intercept velocity, V_i , had been a little smaller, the fit would have been better. The dynamic compressive yield strength reported by Whiffin [2] for electrolytic copper was used for E' in computing V_i for the theoretical curves (see Table 2). It is not known if the electrolytic copper for which Whiffin [2] obtained the dynamic compressive yield strength was equivalent to the electrolytic tough pitch copper that was used for the target plates. Whiffin [2] did not report the static yield strength of the electrolytic copper that he used; he described it as being normally very soft and giving no definite indication of yield point in static compression tests. No formula exists for copper by means of which the dynamic compressive yield strength can be calculated from the static yield strength.

Knowledge of the static yield strength of the copper used for the target plates only provides a means of obtaining comparable data that can be reproduced by other experimenters.

Table 3
Experimental Data^b for Collisions of Mercury Drops with An-
nealed Electrolytic Tough Pitch Copper

0.1-cm drops			0.2-cm drops		
Collision Velocity cm/sec	Drop Diameter cm	Pit Depth cm	Collision Velocity cm/sec	Drop Diameter cm	Pit Depth cm
1.965 x 10 ⁴	0.0946	0.00939	1.773 x 10 ⁴	0.2027	0.02916
1.965	0.0913	0.01016	2.402	0.2002	0.04775
1.965	0.1005	0.01397	2.542	0.2064	0.06604
1.965	0.0966	0.01625	2.7157	0.1989	0.05969
1.978	0.1041	0.016256	2.779	0.1953	0.05867
2.432	0.0976	0.02159	2.8407	0.2030	0.06401
2.829	0.1037	0.02946	2.850	0.2113	0.07467
3.246	0.1054	0.03911	2.865	0.2012	0.06553
3.706	0.1102	0.04445	2.865	0.2012	0.06782
3.761	0.0981	0.04368	2.890	0.2004	0.06502
3.741	0.1070	0.05131	2.984	0.1991	0.07696
4.401	0.1045	0.05867	3.2247	0.2032	0.08229
4.724	0.0991	0.06147	3.310	0.1889	0.07671
5.030	0.0951	0.05994	3.313	0.1951	0.07658
5.371	0.0890	0.06452	3.438	0.2006	0.07366
5.779	0.0956	0.07416	3.575	0.1972	0.09474
6.126	0.1045	0.08356	3.663	0.2032	0.13182
6.486	0.0951	0.08458	3.697	0.1997	0.08357
6.772	0.1041	0.09728	3.786	0.2011	0.12319
7.0896	0.0991	0.09296	4.034	0.2006	0.10731
7.388	0.1010	0.09322	4.096	0.2004	0.11074
7.5255	0.0991	0.09703	4.322	0.2048	0.12268
8.074	0.0935	0.09703	4.401	0.2003	0.12319
8.409	0.1065	0.11684	4.450	0.2025	0.12344
8.708	0.1019	0.11379	4.8615	0.1990	0.1354
9.832	0.1028	0.13894	5.919	0.2099	0.19138
10.500	0.1036	0.13030	6.069	0.2046	0.17919
			6.315	0.2018	0.17754
			6.410	0.1995	0.16992
			6.461	0.1990	0.19990

^b These data were obtained at Convair, Division of General Dynamics Corporation, in San Diego, California. See Reference [1].

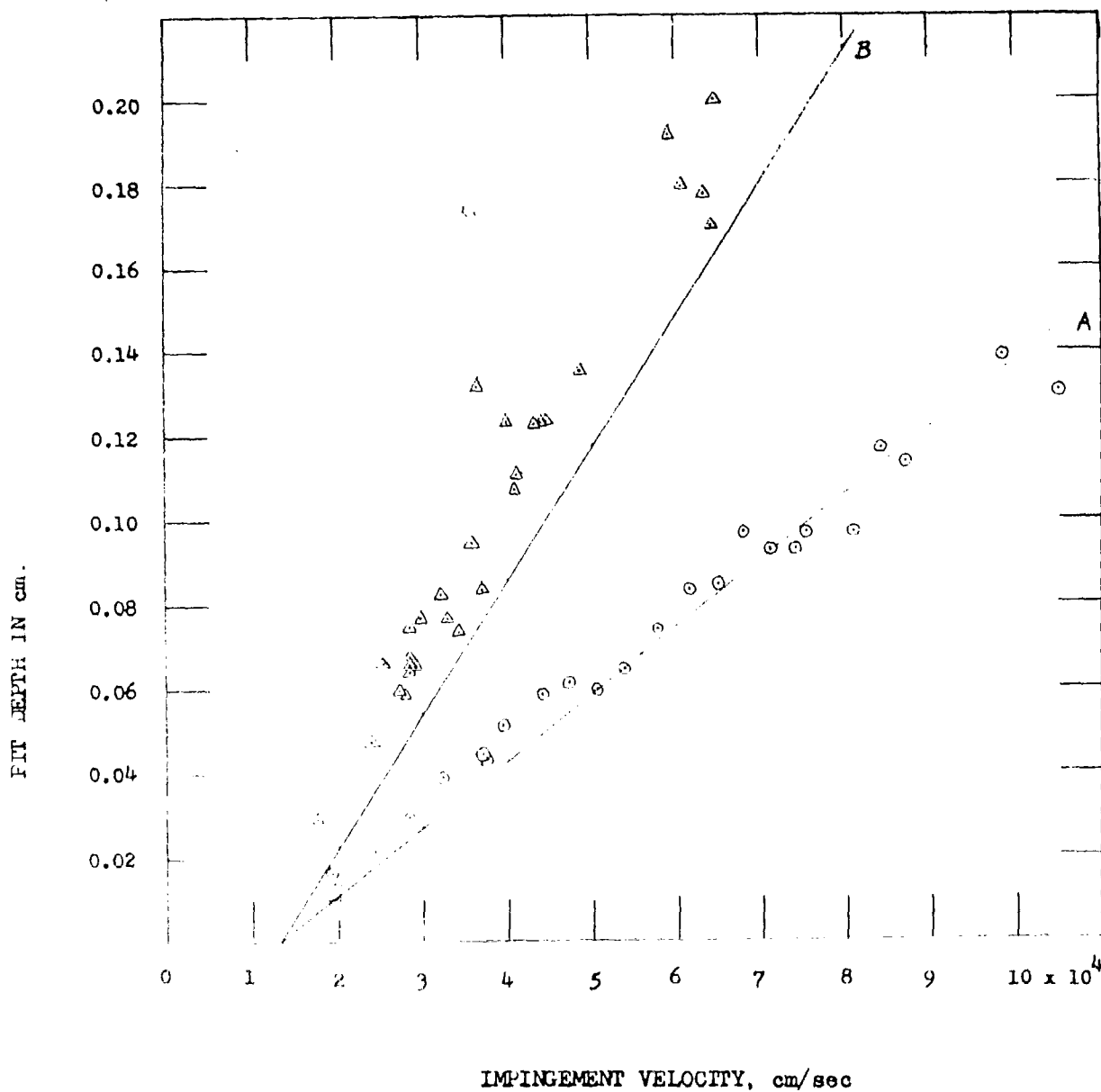


Figure 1. Collisions of Mercury Drops of two sizes against Annealed Electrolytic Tough Pitch Copper

Curve A, calculated with use of Eqs. (1) and (2) for 0.1 -cm drops
 ○, observed depth produced by collision with 0.1 -cm drops
 Curve B, calculated with use of Eqs. (1) and (2) for 0.2 -cm drops
 Δ, observed depth produced by collision with 0.2 -cm drops

The experimental pit depths for collisions of 0.1- and 0.2-cm mercury drops with target plates of 2024-O aluminum are listed in Table 4 and are plotted in Figure 2 with the theoretical curves calculated with use of Eqs (1) and (2) and the data of Table 2.

From Figure 2 it can be seen that the theoretical curves are in reasonably good agreement with the experimental points. As was found to be true in Figure 1, the effect of the change in drop size is properly accounted for by the theoretical equations. As in the case of the copper targets, Curve A, calculated for the 0.1-cm drop size, is in better agreement with the observed depths produced by collision with 0.1-cm drops than Curve B, calculated for the 0.2-cm drop size, is with the observed depths produced by collision with 0.2-cm drops. There is quite a bit of scatter in the experimental points for both drop sizes.

As in the case of the pit-depth-versus-velocity data for copper, there would be better agreement between the theoretical curves and the empirical data if the calculated intercept velocity, V_i , were smaller. In the case of the 2024-O aluminum, the dynamic yield strength that was used for E' in computing V_i was calculated from the measured static yield strength (see Table 2) and should be fairly reliable.

The numerical constants used in Eqs (1) and (2) were originally chosen [1] using pit-depth-versus-velocity data^b for metals whose static yield strength and whose sound speed in infinite medium were not measured experimentally. It is possible that it will be found necessary to change the constants in the equations to some extent when more pit-depth-versus-velocity data become available using targets of metals for which these quantities have been measured.

It is also noteworthy that although Eq (2) appears to be the most acceptable expression for the intercept velocity on the basis of the experimental liquid-drop-versus-solid-target collision data available [1], it is possible that, when more data are obtained and the problem is studied further, it may be found necessary to modify it.

Table 4
Experimental Data^b for Collisions of Mercury Drops
with 2024-0 Aluminum

0.1-cm drops			0.2 - cm drops		
Collision Velocity cm/sec	Drop Diameter cm	Pit Depth cm	Collision Velocity cm/sec	Drop Diameter cm	Pit Depth cm
1.966 x 10 ⁴	0.1032	0.08001	1.7586 x 10 ⁴	0.19514	0.01244
2.454	0.0956	0.02007	2.316	0.19175	0.02718
2.816	0.0940	0.02336	2.554	0.1998	0.03835
2.890	0.1032	0.02562	2.682	0.20122	0.04839
3.413	0.0976	0.03531	2.789	0.1969	0.04902
3.627	0.0996	0.04469	3.048	0.1984	0.05588
3.797	0.1037	0.04902	3.200	0.2017	0.07112
3.822	0.0996	0.04610	3.377	0.19672	0.08560
4.322	0.1037	0.06147	3.596	0.20330	0.09436
4.669	0.1009	0.06756	4.008	0.2047	0.26416
4.745	0.0946	0.05944	4.084	0.2031	0.10947
4.995	0.1041	0.07671	4.517	0.2010	0.25908
5.145	0.1000	0.07722	5.489	0.20572	0.24155
5.517	0.1058	0.09373	5.727	0.2000	0.20650
5.752	0.1014	0.09550	6.834	0.1982	0.26467
6.004	0.0971	0.09906			
6.066	0.0961	0.09677			
6.251	0.1032	0.11252			
6.736	0.1028	0.13080			
7.047	0.0971	0.12408			
7.047	0.0971	0.14986			
7.525	0.1032	0.01333			
8.019	0.1028	0.14656			
8.671	0.1037	0.15977			
8.674	0.1014	0.14884			
8.525	0.1023	0.16650			
8.772	0.1045	0.17627			
9.195	0.0946	0.16281			
9.229	0.0966	0.16357			
9.623	0.1019	0.18288			
10.058	0.0956	0.16256			

^b These data were obtained at Convair, Division of General Dynamics Corporation, in San Diego, California. See Reference [1].

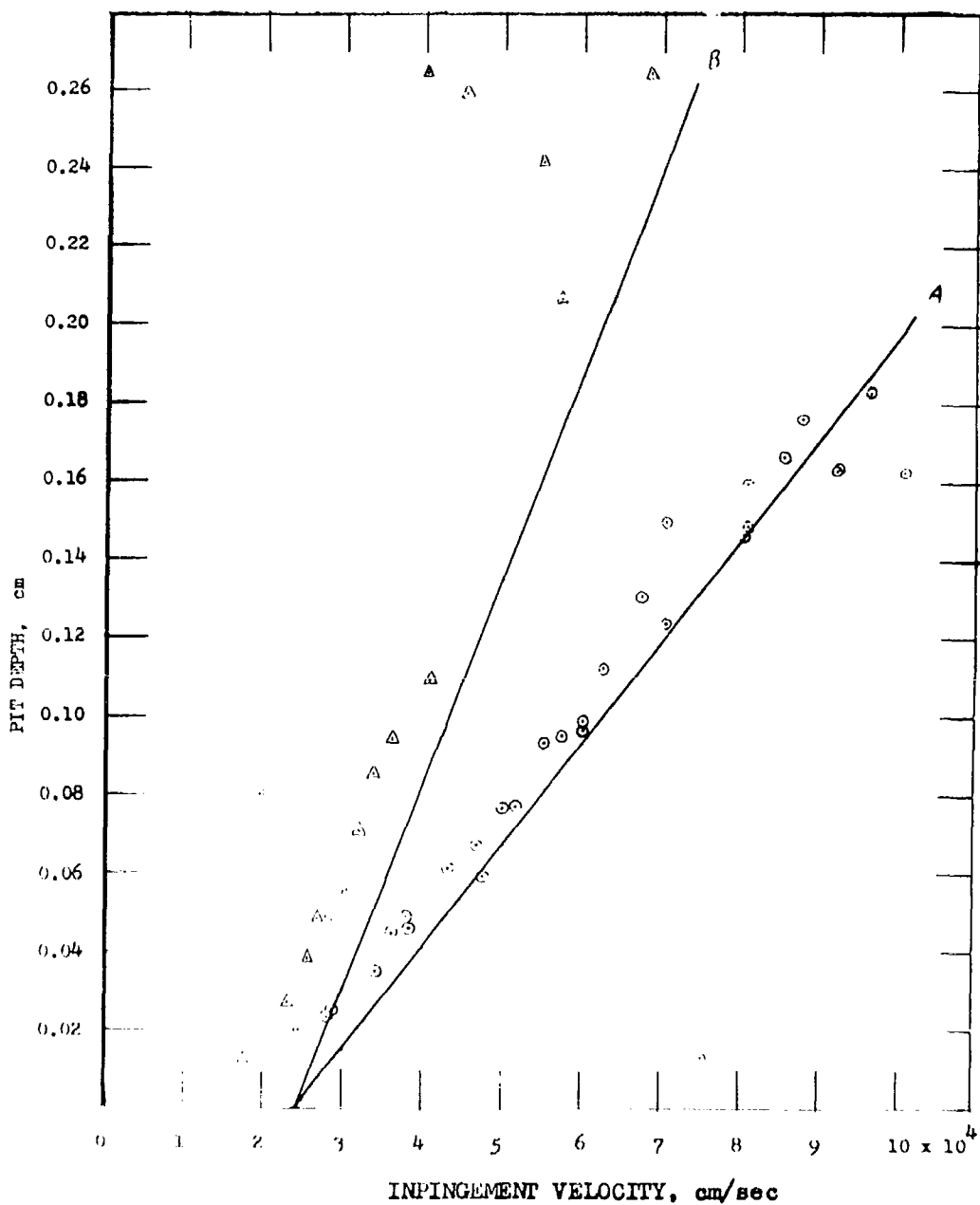


Figure 2. Collisions of Mercury Drops of two Sizes Against 2024-0 Aluminum

Curve A, calculated with use of Eqs (1) and (2) for 0.1 -cm drops

○, observed depth produced by collision with 0.2 -cm drops

Curve B, calculated with the use of Eqs (1) and (2) for 0.2 -cm drops

Δ, observed depth produced by collision with 0.2 -cm drops

2.2 Collisions between Metal Target Plates and Waterdrops

The theoretical curve for collisions of 0.2-cm waterdrops against target plates of annealed electrolytic tough pitch copper is plotted with the experimentally determined pit depths^b in Figure 3. The experimental pit depths are listed in Table 5. The theoretical curve was obtained with use of Eqs (1) and (2) and the data of Table 2. It can be seen from Figure 3 that the theoretical curve is in acceptable agreement both as to slope and intercept with the experimental data that are given. There is, unfortunately, a large amount of scatter in the experimental data which reduces their effectiveness as a check of the theoretical equations.

The theoretical curve for collisions of 0.2-cm waterdrops against target plates of 2024-0 aluminum is shown in Figure 4 along with experimentally determined pit-depth-versus-velocity data^b. The experimental pit depths are listed in Table 6. The theoretical curve was calculated with use of Eqs (1) and (2) and with use of the data of Table 2. From Figure 4 it can be seen that the theoretical curve is a good fit for the experimental data both as to slope and intercept. This is more significant than the extent of agreement found between the theoretical curve and the experimental data in Figure 3 because there is considerably less scatter in these data than in those obtained with the copper targets.

The agreement found between the theoretical curves and the experimental data in Figures 3 and 4 is an indication that Eqs (1) and (2) may be reliable in their present form for calculating the depth of pits that may form in the soft and medium hard metals as a result of collision with liquid drops. Although the speed of sound in mercury is nearly identical with the speed of sound in water, the density, and, therefore, the acoustic impedance, of mercury is very much higher than that of water. Further test of the equations should be made, however, using drops of a liquid that has a sound speed different from that of mercury or water.

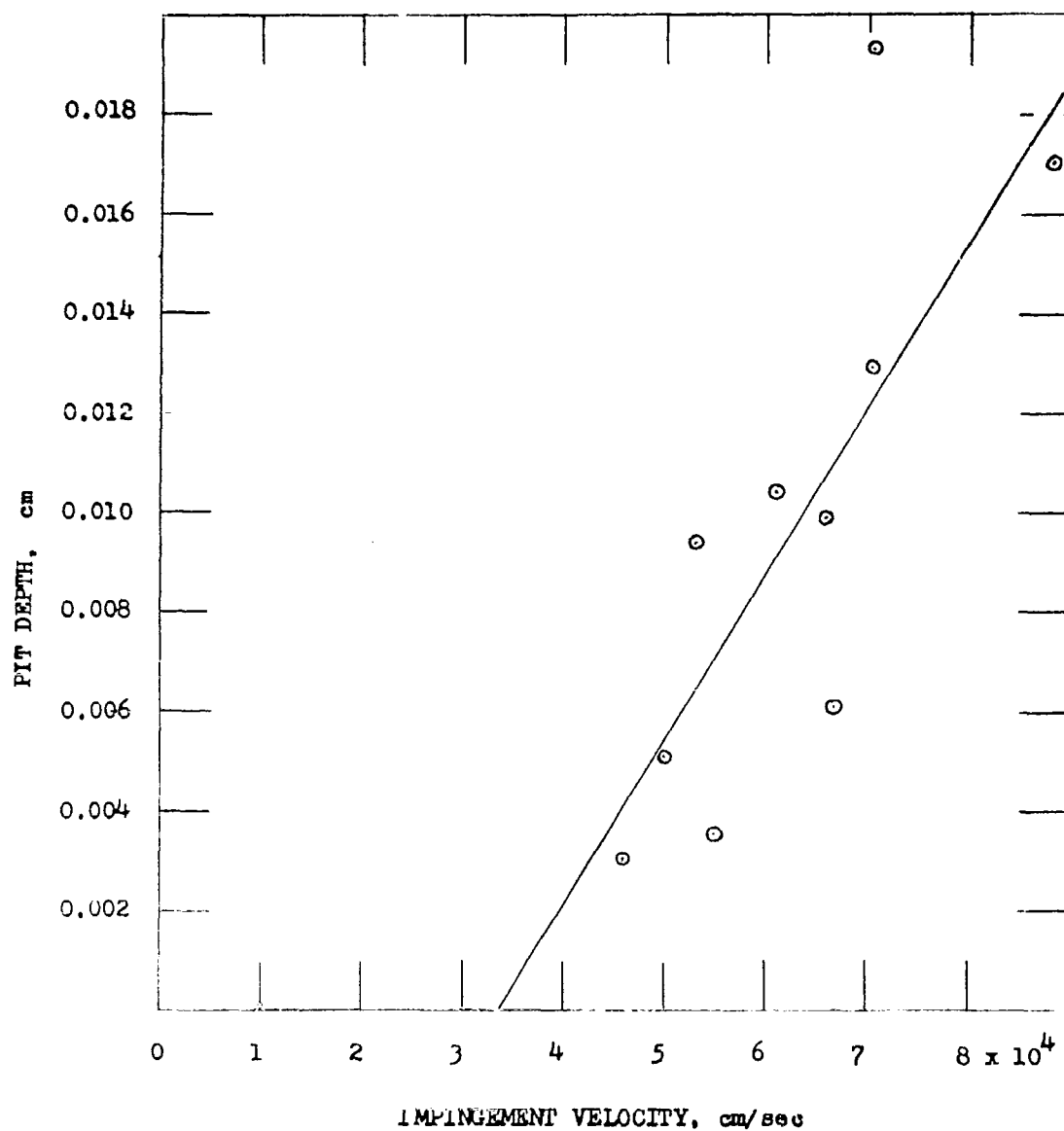


Figure 3. Collisions of 0.2-cm Waterdrops Against Annealed Electrolytic Tough Pitch Copper

— , calculated with use of Eqs (1) and (2) for 0.2-cm drops
 ⊙ , observed depth produced by collision with 0.2-cm drops

Table 5
Experimental Data^b for Collisions of Waterdrops
with Annealed Electrolytic Tough Pitch Copper

Collision Velocity cm/sec	Drop Diameter cm	Pit Depth cm
4.593 x 10 ⁴	0.2	0.00305
4.983		0.00508
5.297		0.00940
5.486		0.00356
6.111		0.01041
6.584		0.00991
6.660		0.00610
7.041		0.01295
7.041		0.01930
8.839		0.01702

Table 6
Experimental Data^b for Collisions of Waterdrops
with 2024-0 Aluminum

Collision Velocity cm/sec	Drop Diameter cm	Pit Depth cm
4.581 x 10 ⁴	0.2	0.00229
4.581		0.00254
4.852		0.00533
5.456		0.00457
6.370		0.01067
6.584		0.01168
7.224		0.01473
7.498		0.02057

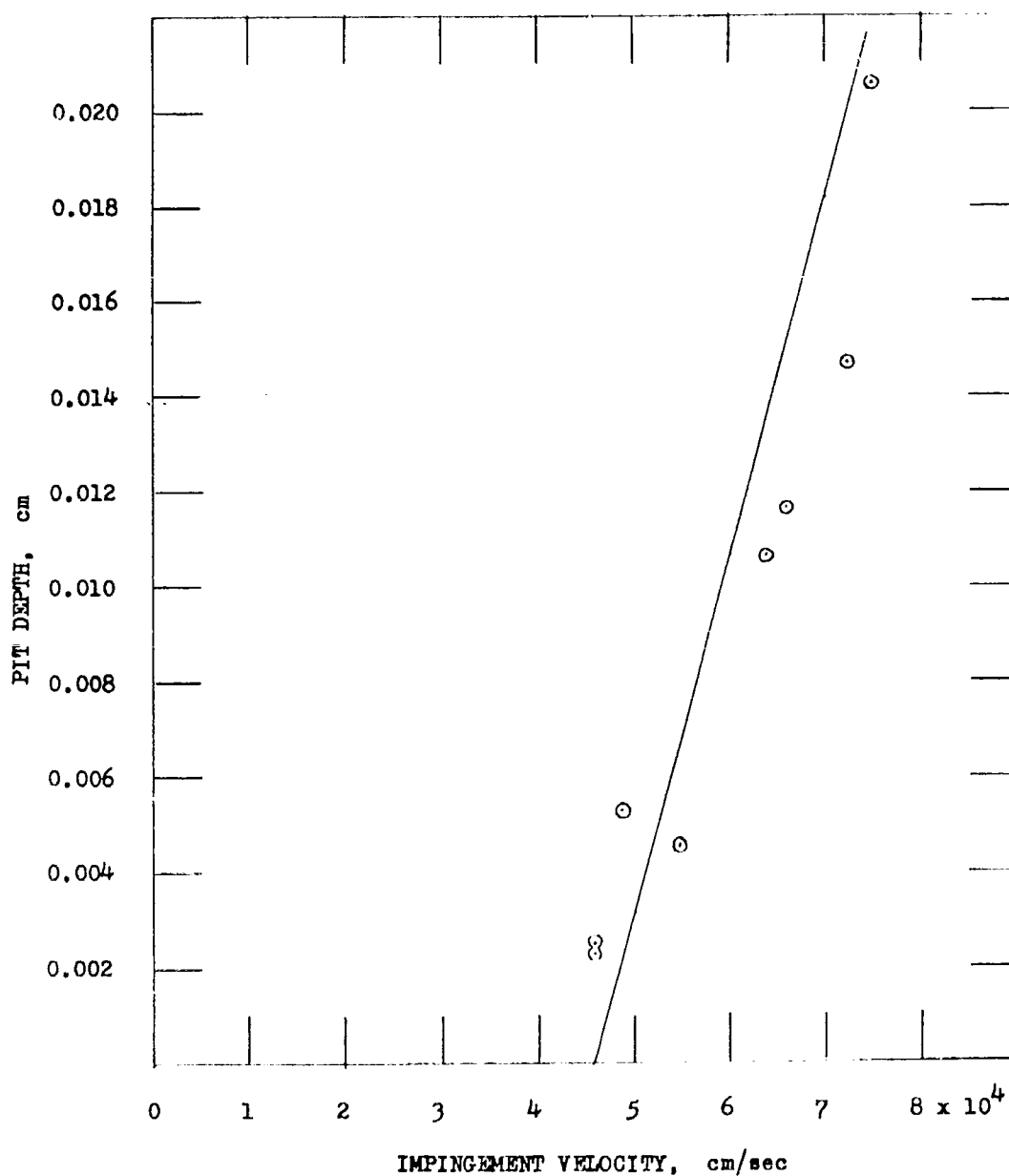


FIGURE 4. COLLISIONS OF 0.2-cm WATERDROPS AGAINST 2024-O ALUMINUM

—————, calculated with use of Eqs (1) and (2) for 0.2-cm drops

(○), observed depth produced by collision with 0.2-cm drops

3. Solid-Versus-Solid Collisions

Because the pit-depth-versus-velocity equation that was developed [1] for collisions of metal target plates with liquid drops ignored such characteristic fluid-flow parameters as the Weber Number and the Reynolds Number, it should apply equally well to pits produced by collision of solid spheres with target plates of the soft and medium hard metals. The equation may, in fact, be substantiated further with data of this kind.

To explore this possibility, 1-in.-thick plates of 1100-0 aluminum, 2024-0 aluminum, and annealed electrolytic tough pitch copper were used as targets for steel sphere impingement at the U. S. Naval Research Laboratory in Washington, D. C. The test firings were made under the direction of Mr. Wilfred J. Ferguson and Mr. Harry O. Ewing.

The shots were made using a target mounting in which the plate was given edge support only. In this form of mounting the rear face of the target plate was a free surface. These data are presented and discussed in Sections 3.1, 3.2, and 3.3. One set of data for collisions of steel spheres against 2024-0 aluminum target plates was collected with the aluminum alloy plate backed with a 5-x-6-in. steel supporting block that was three inches thick. In this form of mounting the rear face of the target plate was not a free surface. These data are presented and discussed in Section 3.4.

The velocity measurements were made with use of a Potter chronograph. The base length was 12 inches. The chronograph was started and stopped by breaking conducting grids. The distance from the midpoint of the base length to the target face was 23 inches; the velocity measurements were not corrected for deceleration of the steel spheres during transit over this distance.

The steel spheres that were used in making the shots were SKF Grade 1. They had an approximate hardness of 60 on the Rockwell C scale. These spheres have a high order of accuracy in dimensions because they are made for ball bearings. Three sphere sizes were used for the firings: 7/32-in. , 5/16-in. , and 1/2-in. diameter.

The depths of the pits that were produced by impingement of the steel spheres against target plates of the three metals that were used were measured with use of an Ames dial gauge that was graduated in mils. Each depth measurement is the difference between the dial reading at the pit bottom and an average of four dial readings taken on the surface of the target plate around the mouth of the crater.

3.1 Collisions of Steel Spheres with Target Plates of 1100-0 Aluminum

The velocity at which the shots were made and the depths of the pits that were produced by the shots in the 1100-0 aluminum plates are given in Table 7 for the three sizes of steel spheres that were used.

The pit-depth-versus-velocity curve for collisions of steel spheres with 1100-0 aluminum was first calculated according to the equations that were developed for collisions between metal target plates and liquid drops. Although the experimental pit-depth-versus-velocity data were found to lie along straight lines, the slope of the lines was found to be much steeper than that of the lines given by the pit-depth-versus-velocity equation for collision of liquid drops against target plates of the soft and medium hard metals. This is logical and should have been expected because in the case of the very hard steel-sphere projectiles most of the collision energy is used in forming the pits whereas in the case of the projectiles that flow during and as a result of the collision part of the collision energy is used in the flow of the projectile.

Table 7
Experimental Data^k for Collisions of
Steel Spheres with 1100-O Aluminum

Sphere Diameter 0.5556 cm (7/32 in.)		Sphere Diameter 0.7938 cm (5/16 in.)		Sphere Diameter 1.270 cm (1/2 in.)	
Velocity cm/sec	Pit Depth cm	Velocity cm/sec	Pit Depth cm	Velocity cm/sec	Pit Depth cm
0.9784 x 10 ⁴	0.0998	0.7163 x 10 ⁴	0.110	0.887 x 10 ⁴	0.224
1.018	0.104	0.9723	0.146	1.055	0.272
1.049	0.107	1.265	0.192	1.295	0.329
1.411	0.148	1.414	0.212	1.558	0.375
1.457	0.151	1.490	0.224	1.609	0.392
1.704	0.180	1.506	0.234	1.759	0.448
1.871	0.199	1.530	0.234	1.807	0.466
2.140	0.229	1.646	0.253	2.009	0.526
2.146	0.233	1.661	0.256	2.082	0.556
2.576	0.291	1.783	0.276	2.121	0.608
2.865	0.344	1.789	0.275	2.128	0.554
3.103	0.373	1.862	0.297	2.414	0.656
		1.993	0.317		
		2.137	0.341		
		2.423	0.378		

These data were obtained at the U. S. Naval Research Laboratory
in Washington, D. C.

To fit the experimental data, it was found by trial that it was necessary to increase the numerical constant in the expression for pit depth to 17.5 and to reduce the numerical constant in the expression for the intercept velocity to 1. With these changes, the pit-depth-versus-velocity equation for collisions of projectiles that neither flow nor undergo appreciable permanent yield with targets of the soft and medium hard metals is

$$\delta' = \left[17.5 d z / c(z + z') \right] \cdot \left[V - V_1 \right] \quad (3)$$

where

$$V_1 = E' (z + z') / (\rho c' z'^3)^{1/2} \quad (4)$$

The theoretical pit-depth-versus-velocity curves, calculated by use of Eqs (3) and (4) with the data given in Table 2, for collisions of steel spheres of three sizes against 1100-0 aluminum target plates are shown with the experimentally determined points in Figure 5. From Figure 5 it can be seen that the experimental points follow the theoretical curves. In particular, it can be seen that the effect of a change in sphere size is properly accounted for by the equations.

3.2 Collisions of Steel Spheres with Target Plates of Annealed Electrolytic Tough Pitch Copper

The velocity at which the shots were made and the depth of the pits that were produced by the shots with three sizes of steel spheres against 1-in.-thick plates of annealed electrolytic tough pitch copper are given in Table 3. Theoretical pit-depth-versus-velocity curves calculated by use of Eqs (3) and (4) with the material constants given in Table 2 are shown with the experimentally determined points in Figure 6. From Figure 6 it can be seen that there is quite a bit of scatter in the experimental data for the 1/2-in.-diameter steel spheres. Nevertheless, there is, in general, good agreement between the theoretical curves and the observed points. From Figure 6 it can be seen that the effect of a change in sphere size is properly accounted for by the equations.

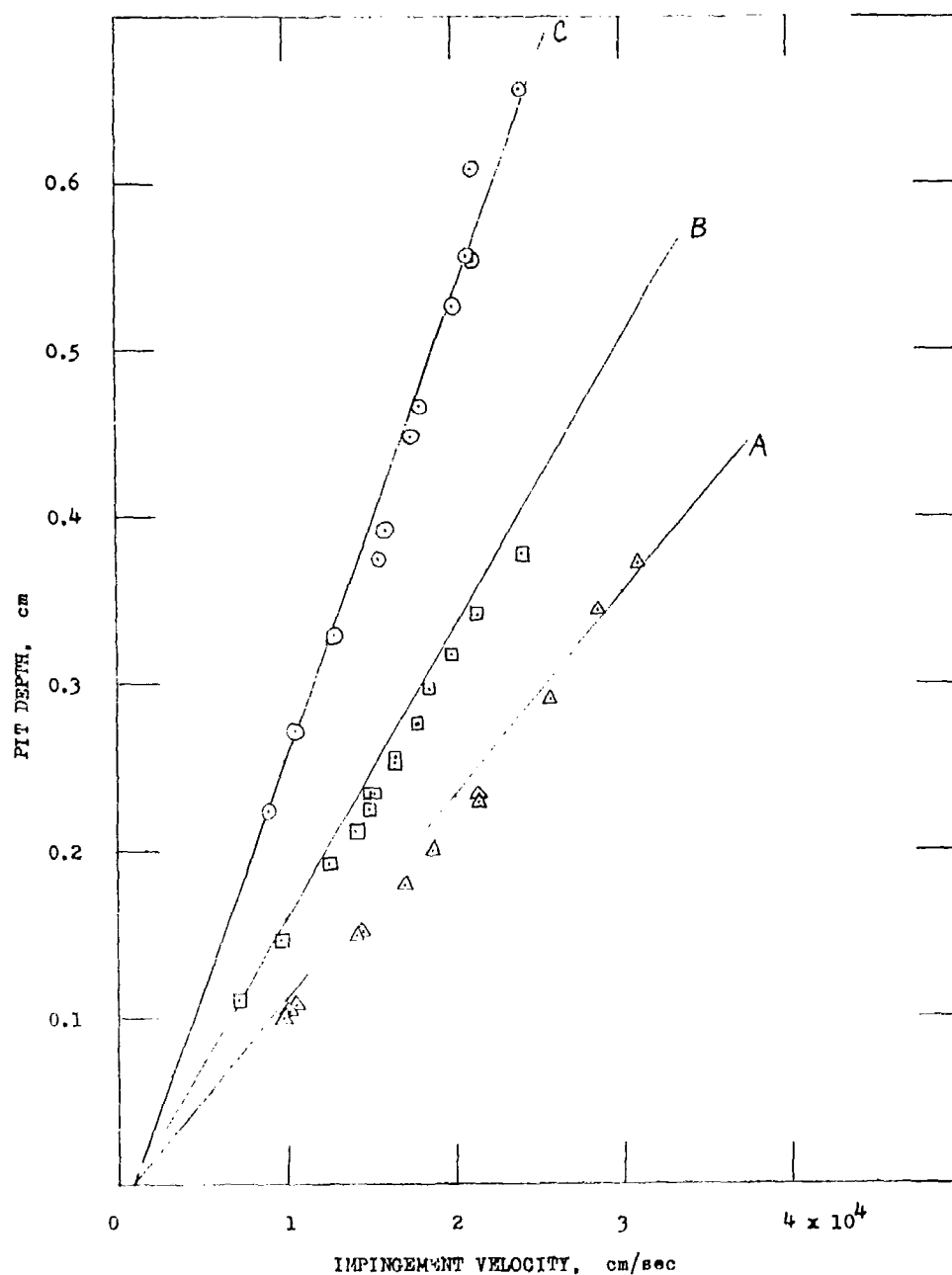


FIGURE 5. COLLISIONS OF STEEL SPHERES OF THREE SIZES AGAINST 1100-O ALUMINUM

- Curve A, calculated with use of Eqs (3) and (4) for 7/32-in. spheres
- Δ , observed depth produced by collision with 7/32-in. spheres
- Curve B, calculated with use of Eqs (3) and (4) for 5/16-in. spheres
- \square , observed depth produced by collision with 5/16-in. spheres
- Curve C, calculated with use of Eqs (3) and (4) for 1/2-in. spheres
- \circ , observed depth produced by collision with 1/2-in. spheres

Table 8
Experimental Data^k for Collisions of Steel Spheres
with Annealed Electrolytic Tough Pitch Copper

Sphere Diameter 0.5556 cm (7/32 in)		Sphere Diameter 0.7938 cm (5/16 in)		Sphere Diameter 1.270 cm (1/2 in)	
Velocity cm/sec	Pit Depth cm	Velocity cm/sec	Pit Depth cm	Velocity cm/sec	Pit Depth cm
1.100 x 10 ⁴	0.0869	0.7803 x 10 ⁴	0.0902	0.4084 x 10 ⁴	0.0828
1.372	0.103	0.9388	0.109	0.4389	0.0917
1.500	0.154	1.119	0.124	0.9601	0.184
1.878	0.138	1.283	0.145	1.353	0.240
1.981	0.145	1.588	0.173	1.411	0.249
2.121	0.156	1.740	0.188	1.426	0.250
2.124	0.159	2.280	0.249	1.451	0.309
2.158	0.167	2.377	0.262	1.868	0.301
2.225	0.166	2.457	0.274	1.966	0.354
2.234	0.166			2.036	0.369
2.256	0.170			2.060	0.377
2.271	0.172			2.134	0.425
2.316	0.176			2.204	0.395
2.646	0.202			2.216	0.400
2.685	0.206			2.694	0.573
2.960	0.233			2.704	0.388
3.560	0.280			3.066	0.580
				3.109	0.495
				3.225	0.622
				3.432	0.638

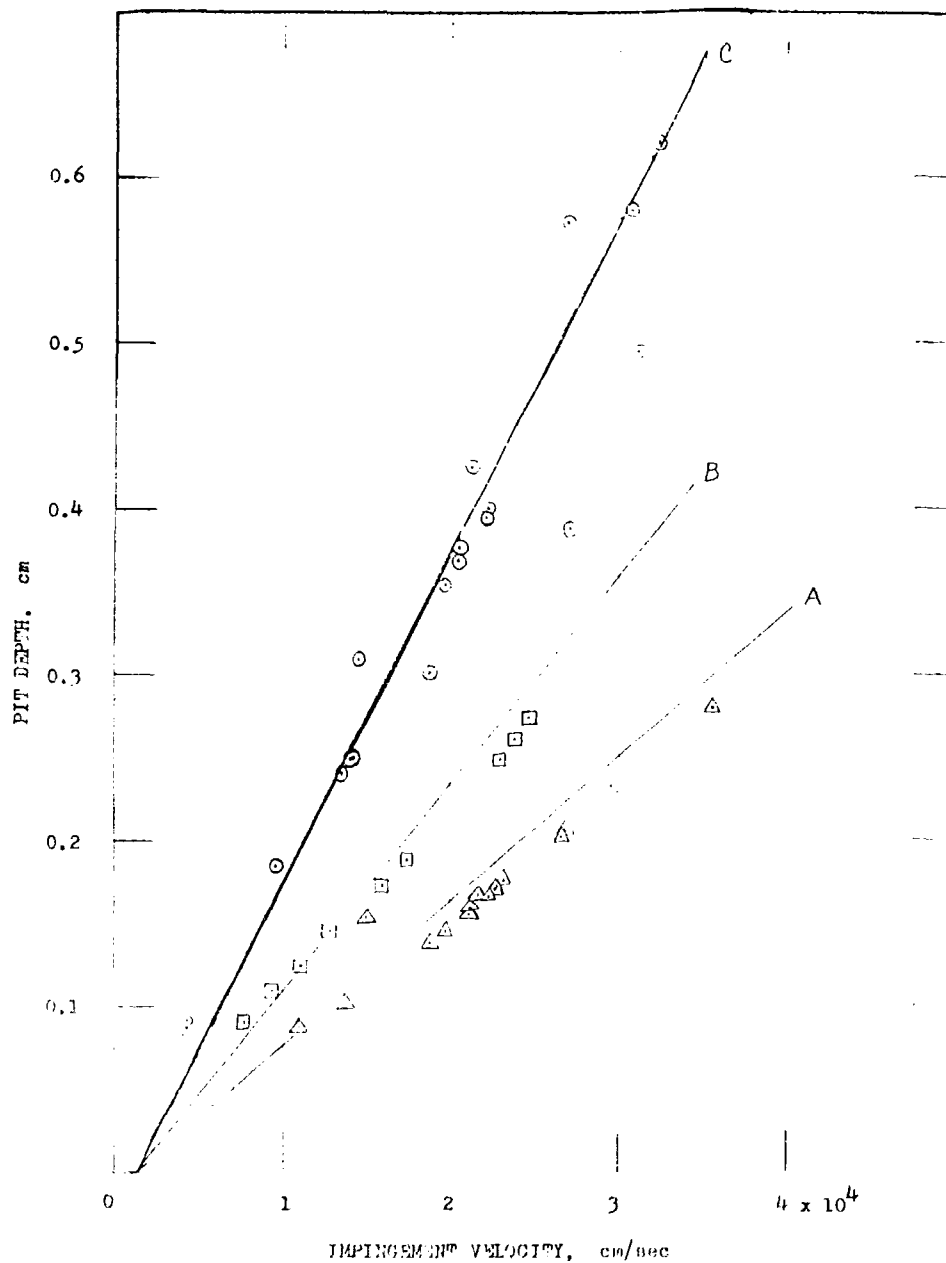


FIGURE 6. COLLISIONS OF STEEL SPHERES OF THREE SIZES AGAINST ANNEALED ELECTROLYTIC TOUGH PITCH COPPER

- Curve A, calculated with use of Eqs (3) and (4) for 7/32-in. spheres
 Δ , observed depth produced by collision with 7/32-in. spheres
 Curve B, calculated with use of Eqs (3) and (4) for 5/16-in. spheres
 \square , observed depth produced by collision with 5/16-in. spheres
 Curve C, calculated with use of Eqs (3) and (4) for 1/2-in. spheres
 \circ , observed depth produced by collision with 1/2-in. spheres

3.3 Collisions of Steel Spheres with Target Plates of 2024-O Aluminum

The velocity at which shots with three sphere sizes were made against target plates of 2024-O aluminum and the depth of the pits that were produced by the shots are given in Table 9. Theoretical pit-depth-versus-velocity curves were calculated by use of Eqs (3) and (4) with the material constants given in Table 2. These curves are plotted with the experimental data in Figure 7. It can be seen from Figure 7 that for each sphere size that was used, the experimental points lie below the theoretical curve.

It was thought at first that the reason for this discrepancy might be that in steel-sphere collisions with materials that are as strong as 2024-O aluminum the steel sphere may be permanently deformed and that in this way part of the collision energy may be diverted from pit formation whereas in the case of the very soft metals all of the collision energy may go into pit formation. Later, in view of the information that heat-treated 2024-O aluminum is subject to spalling, it was thought that energy may be diverted from pit formation into crack formation although this is unlikely in the case of the annealed metal. Finally, the explanation for the discrepancy was sought in the extent to which sound is attenuated in the target metals, and in the ability of the target metals to work-harden.

To check the first possibility, two 1/2-in.-diameter steel spheres that were fired against targets of annealed copper and 2024-O aluminum, respectively, were recovered. The sphere that struck the copper target had a collision velocity of 1,126 ft/sec and the sphere that struck the 2024-O aluminum target had a collision velocity of 1,200 ft/sec. These spheres were examined with a microinterferometer in NPS Engineering Metrology Section. It was found that the diameter measured through the impact area of the sphere that was shot into copper was 0.0010 in. smaller than diameters measured outside of the impact area and that the diameter measured through the impact area of the sphere that was shot into 2024-O aluminum was 0.00008 in. smaller than diameters measured outside of the impact area. On the basis of this evidence it cannot be concluded that a larger

Table 9
Experimental Data^k for Collisions of Steel Spheres
with 2024-O Aluminum

Sphere Diameter 0.5556 cm (7/32 in)		Sphere Diameter 0.7938 cm (5/16 in)		Sphere Diameter 1.270 cm (1/2 in)	
Velocity cm/sec	Pit Depth cm	Velocity cm/sec	Pit Depth cm	Velocity cm/sec	Pit Dep cm
1.113×10^4	0.0790	0.7894×10^4	0.0800	0.5578×10^4	0.197
1.451	0.103	1.067	0.107	0.5822	0.172
1.542	0.109	1.305	0.149	1.207	0.197
1.981	0.135	1.698	0.173	1.326	0.268
2.173	0.156	1.771	0.180	1.460	0.248
2.274	0.188	1.832	0.185	2.039	0.345
2.368	0.169	2.856	0.349	2.722	0.482
2.448	0.178			2.780	0.493
2.701	0.197			2.786	0.491
				3.301	0.622
				3.484	0.360
				3.548	0.622
				3.658	0.606

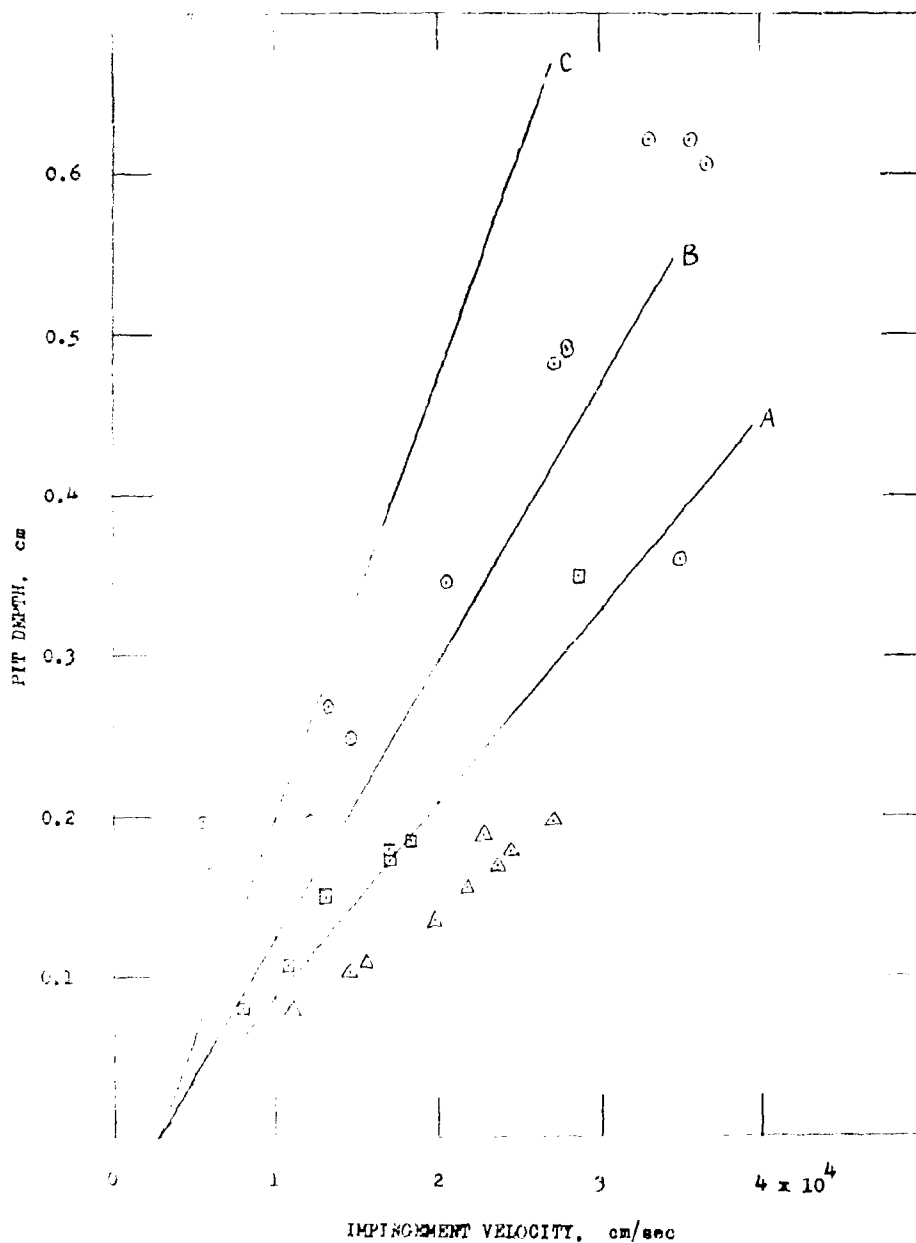


FIGURE 7. COLLISIONS OF STEEL SPHERES OF THREE SIZES AGAINST 2024-O ALUMINUM

- Curve A, calculated with use of Eqs (3) and (4) for 7/32-in. spheres
- , observed depth produced by collision with 7/32-in. spheres
- Curve B, calculated with use of Eqs (3) and (4) for 5/16-in. spheres
- , observed depth produced by collision with 5/16-in. spheres
- Curve C, calculated with use of Eqs (3) and (4) for 1/2-in. spheres
- △, observed depth produced by collision with 1/2-in. spheres

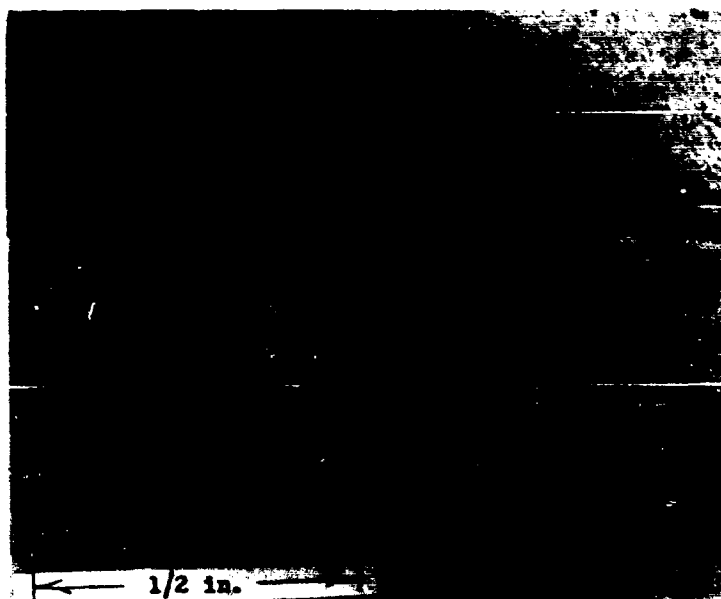
percentage of the impact energy is absorbed by a steel sphere on colliding with 2024-0 aluminum than on colliding with annealed copper. In fact, the reverse is the case. Deformation of the steel sphere is not the cause of the divergence of the 2024-0 aluminum experimental pit-depth-versus-velocity data from the theoretical curves.

Cross-sectional cuts were then made of the pits produced by these spheres. These were mounted in plastic in NBS Mechanical Metallurgy Section. They were given a high polish. See Figure 8. They were examined with a microscope for evidence of crack formation. No reliable evidence of crack formation was found. The cross section of the pit in 2024-0 aluminum was then etched in an effort to accentuate any cracks if they existed, but no bona fide cracks were found. Crack formation in the target is, therefore, not the cause of the divergence of the 2024-0 aluminum experimental pit-depth-versus-velocity data from the theoretical curves.

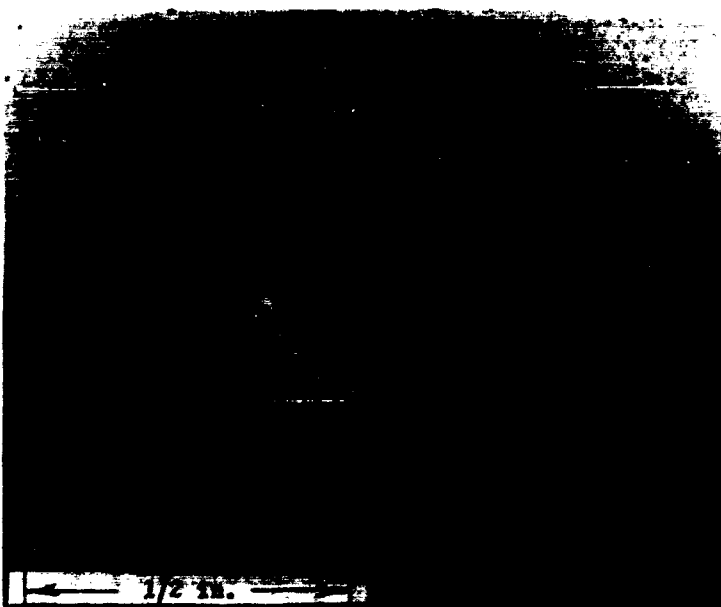
It was then thought that the compressional wave caused by the collision may have reflected from the free reverse surface of the 2024-0 aluminum target plate as a tension wave and may have returned to the collision surface with the effect of filling in the pits. This possibility is in agreement with the fact that attenuation of sound is greater in 1100-0 aluminum and in annealed copper than it is in 2024-0 aluminum.

To test this possibility a 5/8-in.-thick plate of 1100 aluminum was cut to fit one of the 1-in.-thick target plates of 2024-0 aluminum and was annealed under the same conditions as those that were used for the 1100-0 aluminum targets. The contact surfaces between the two plates were machine ground and polished until, when they were pressed together, one plate was able to lift the other. These plates were sent to the Naval Research Laboratory; they were tightly clamped together and eleven test firings were made against the combination target plate. The reverse (1100-0 aluminum) face of the combination target plate was maintained as a free surface during the firings. Steel spheres that were 5/16 inch in diameter were used for the shots.

It was hoped that if the compressional waves produced by the collisions had been returning to the collision surface as tension waves they would now be prevented from doing this by attenuation on transit through the 1100-0 aluminum. However,



Pit in
Aluminum Alloy



Pit in
Copper

FIGURE 8. Cross Sections of Pits Produced by Collision of a 1/2-in.
Steel Sphere with Annealed Electrolytic Tough Pitch
Copper and with 2024-0 Aluminum

when the pit depths were measured and when the measured pit depths were plotted against the impingement velocity, it was found that the points were in complete agreement with those obtained without the 1100-0 aluminum backing plate. The pit-depth-versus-velocity data are given in Table 10. Apparently the return of the reflected tension wave to the collision surface is unable to explain the divergence of the 2024-0 aluminum pit-depth-versus-velocity data from the theoretical curves.

The explanation was finally sought in the work-hardening properties of the three metals that were used as targets. When a rigid sphere impinges against a metal target plate, shear stresses exist around the cylinder of target metal that is set in motion as a result of the collision as indicated by the arrows marked τ_A in Figure 9. Shear stresses also exist in the target metal around the point of impingement as indicated by the arrows marked τ_B in Figure 9. It seems reasonable that, if the metal does not work-harden readily, or if the τ_B -shear stress is small, most of the plastic flow that takes place will occur as a result of the shear stress τ_A around the cylinder of target metal that exists below the collision area. If, however, the metal work-hardens extensively while this process is initiated, flow as a result of the shear stress τ_A will be inhibited. In this case flow will occur as a result of the shear stress τ_B , if the τ_B -shear stress is appreciable, and the surface of the metal will be raised in a ring around the mouth of the pit that forms as a result of the collision.

It can be seen by laying a straight edge across the mouths of the craters shown in Figure 8 that there is a considerable elevation of the target metal around the crater in the case of the 2024-0 aluminum. Visual inspection of the target plates revealed that there was some rising of metal around the craters, especially in the case of the largest sphere size, for each of the target metals used. It seemed, however, to have occurred to a somewhat greater degree in the case of the 2024-0 aluminum than in the case of the 1100-0 aluminum or of the annealed electrolytic tough pitch copper.

Equations (1), (2), (3), and (4) were developed [1] on the assumption that the principal movement that occurs as a result of a liquid-drop or of a steel-sphere collision with a

Table 10
 Experimental Data^k for Collisions of 5/16-in. Steel Spheres
 with a
 2024-0 Aluminum and 1100-0 Aluminum Combination Target

Collision Velocity cm/sec	Pit Depth cm
0.9601×10^4	0.0955
1.201	0.1204
1.478	0.1488
1.646	0.1659
1.890	0.1933
2.103	0.2217
2.603	0.2802
2.734	0.2967
2.841	0.2941
3.203	0.3663
3.755	0.4534

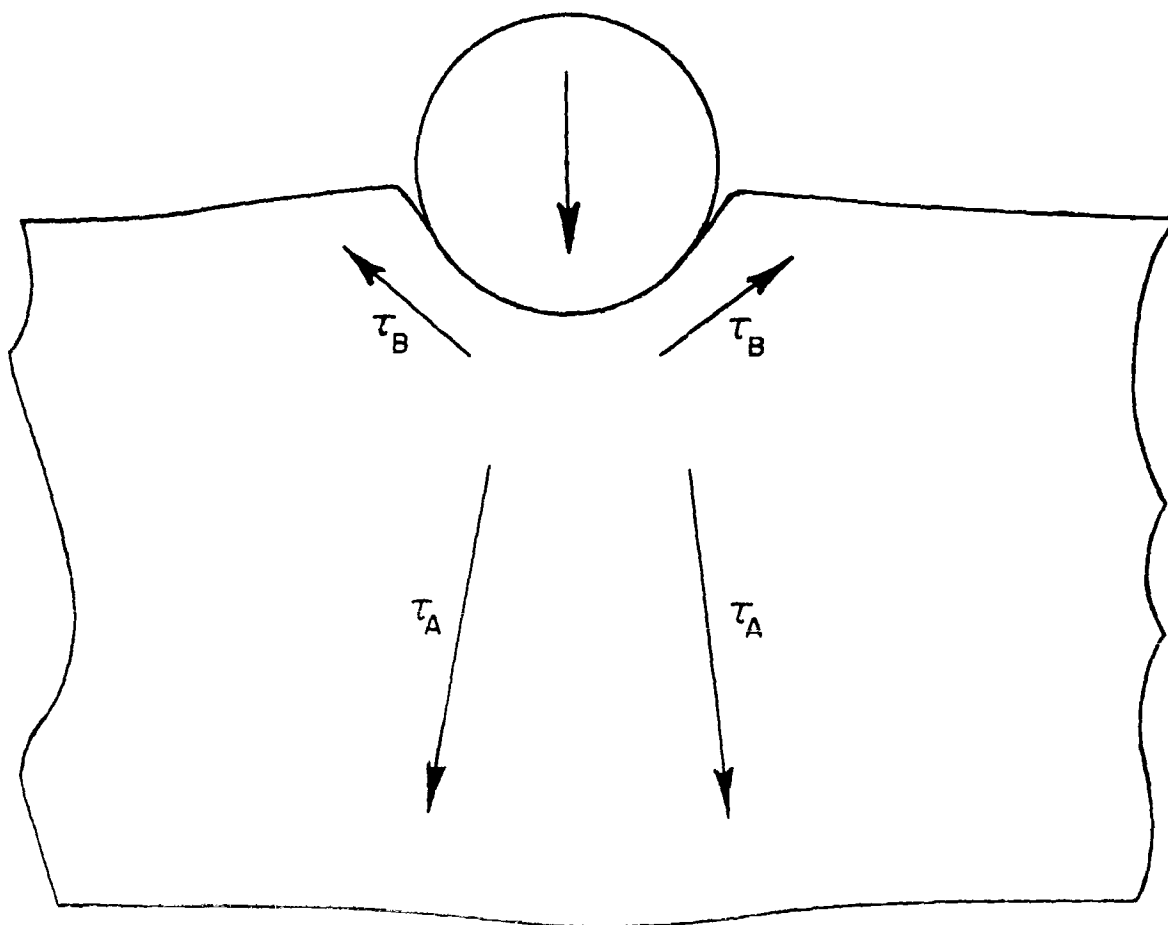


Figure 9. Shear Stresses Produced in a Metal Plate by an Impinging Steel Sphere.

metal target plate is that of the core of metal under the collision area. If any other flow process (such as that resulting from the shear stress τ_B of Figure 9) becomes appreciable in a specific target metal, these equations cannot be expected to apply to pits formed in that metal.

A comparison of the work-hardening properties of the 1100-0 aluminum, annealed electrolytic tough pitch copper, and 2024-0 aluminum, which were used in the collision experiments, was made by referring to the engineering stress-strain curves. These curves, made from data that were obtained when the tensile specimens were tested (See Section 1.2), are plotted in Figure 10. The slopes of the curves for the three metals in the range of strain from 0.003 to 0.004 inch per inch are 226,000 psi, 553,000 psi, and 921,000 psi, respectively. From these data it can be concluded that the 2024-0 aluminum work-hardens much more than does the annealed electrolytic tough pitch copper or the 1100-0 aluminum. Copper is the main alloying element in 2024-0 aluminum. Thomas and Nutting [5] have also found that aluminum-copper alloys that were given a 4-hour soak at 535°C followed by water quenching work-hardened more than pure aluminum that was annealed for 3 hours at 600°C.

The work-hardening behavior of the three metals used for the experiments is in agreement with the fact that the pit-depth-versus-velocity data for 1100-0 aluminum and for annealed electrolytic tough pitch copper are well fitted by the theoretical curves calculated with use of Eqs (3) and (4) whereas those for 2024-0 aluminum are not. It is possible that the plastic yield that occurs in 1100-0 aluminum and in annealed electrolytic tough pitch copper as a result of impingement of steel spheres may be caused almost entirely by the shear stress τ_A in Figure 9 whereas the plastic yield that occurs in 2024-0 aluminum as a result of impingement of steel spheres may be caused both by the shear stress τ_A and the shear stress τ_B in Figure 9.

For mercury-drop and waterdrop impingement the pit-depth-versus-velocity data for 2024-0 aluminum were well fitted by the theoretical curves calculated with use of Eqs (1) and (2). See Figures 2 and 4. This is not a contradiction because it is likely that the τ_B -shear stress of Figure 9 is smaller for the case of projectiles that flow during and as a result of the collision than for the case of projectiles that do not flow.

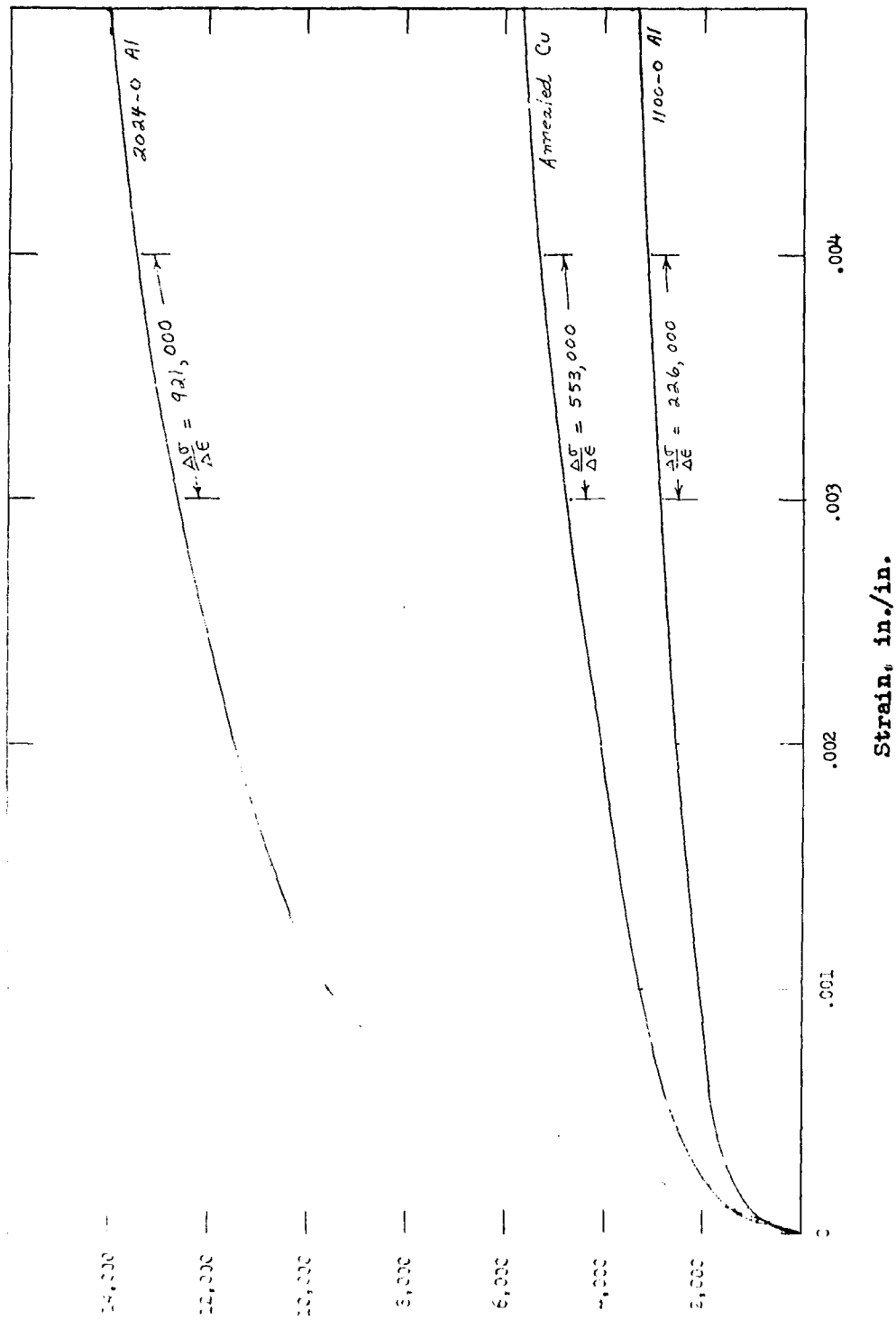


Figure 10. Stress-Strain Curves for 1100-0 Aluminum, 2024-0 Aluminum, and Annealed Electrolytic Tough Pitch Copper.

More data, using steel-shere projectiles and target metals that have different work-hardening properties, are needed to prove whether or not the analysis that has been made is correct.

3.4 Collisions of Steel Spheres with Target Plates of 2024-0 Aluminum that Were Backed with a Heavy Steel Supporting Block

It has been pointed out that Eqs (1), (2), (3), and (4) only apply to the case that the target plate has edge support during the firings; the reverse side of the target plate must be a free surface. This is because the model on which Eqs (1), (2), (3), and (4) are based involves the movement of the core of target material under the collision area with respect to the remainder of the target plate. See Reference [1]. If the target plate is backed by a heavy metal plate or block, the reverse face of the target plate is not a free surface, the core of material under the collision area is not free to move with respect to the remainder of the target plate, and Eqs (1), (2), (3), and (4) do not apply.

Pit-depth-versus-velocity data were obtained for collisions of steel spheres of three sizes against 1-in.-thick target plates of 2024-0 aluminum that were backed with a 5-x-6-in. steel supporting block that was three inches thick. These data are of no value as far as substantiating Eqs. (1), (2), (3), and (4) is concerned. They are presented in this section to show how the pit-depth-versus-velocity curve differs for the two modes of support of the target plate during the firings.

The experimental pit-depth-versus-velocity data that were obtained for collisions of three sizes of steel spheres against 2024-0 aluminum targets that were backed with a steel block are listed in Table 11. They are plotted in Figure 11 where best-fit curves have been drawn through the data for each size of steel sphere that was used. It can be seen from Figures 7 and 11 that when the reverse side of the target plate is a free surface, the pit-depth-versus-velocity curve is a straight line, but that when the reverse side of the target plate is not a free surface (use of a backing plate or block), the pit-depth-versus-velocity curve is not a straight line.

Table 11
Experimental Data^k for Collisions of Steel Spheres with
2024-0 Aluminum Backed with a Steel Supporting Block

Sphere Diameter 0.5556 cm (7/32 in.)		Sphere Diameter 0.7938 cm (5/16 in.)		Sphere Diameter 1.270 cm (1/2 in.)	
Velocity cm/sec	Pit Depth cm	Velocity cm/sec	Pit Depth cm	Velocity cm/sec	Pit Depth cm
1.106 x 10 ⁴	0.0742	0.6035 x 10 ⁴	0.0991	0.9753 x 10 ⁴	0.160
1.192	0.0803	1.012	0.115	0.9845	0.162
1.295	0.0866	1.186	0.147	1.341	0.230
1.548	0.106	1.247	0.121	1.664	0.283
1.844	0.127	1.356	0.117	1.966	0.332
2.027	0.141	1.369	0.133	2.094	0.370
2.115	0.146	1.384	0.135	2.143	0.374
2.298	0.165	1.384	0.136	2.146	0.375
2.408	0.174	1.417	0.133	2.502	0.438
2.438	0.179	1.436	0.140	2.697	0.512
2.502	0.182	1.481	0.139	2.780	0.495
2.609	0.187	1.503	0.149	3.283	0.618
2.615	0.193	1.622	0.157	4.331	0.461
2.615	0.188	1.786	0.178		
2.688	0.198	1.823	0.184		
3.036	0.231	1.939	0.197		
3.216	0.252	2.057	0.211		
		2.216	0.230		
		2.640	0.287		
		3.255	0.372		
		3.572	0.416		
		4.209	0.529		
		4.846	0.646		

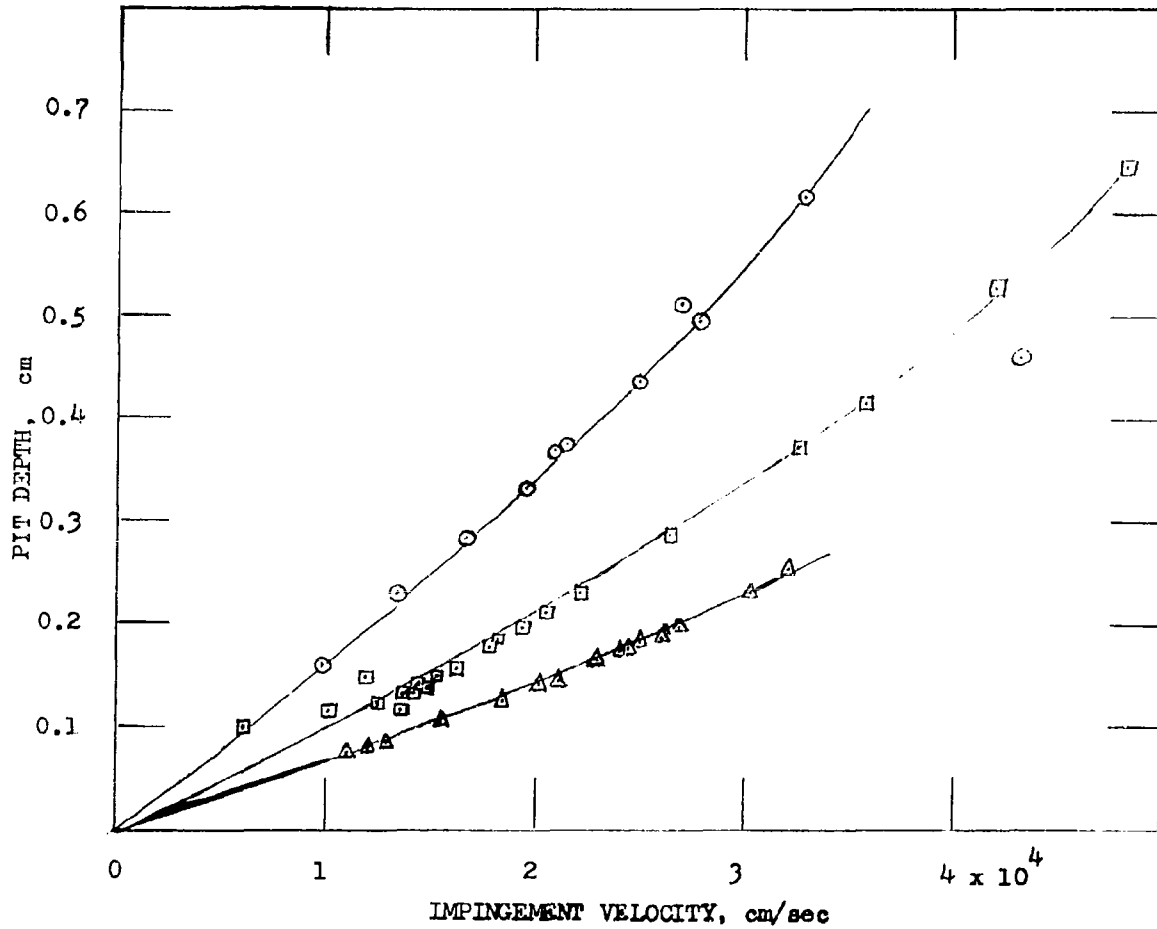


Figure 11. Best-fit Curves for Collisions of Steel Spheres Against 2024-0 Aluminum Targets Backed with Heavy Steel Supporting Block

- Δ , observed depth produced by collision with 7/32-in.spheres
- \square , observed depth produced by collision with 5/16-in. spheres
- \circ , observed depth produced by collision with 1/2-in. spheres

For the case that the reverse face of the target plate is a free surface, the projectile is stopped by the resistance of the target metal to shear. For the case that the reverse face of the target plate is not a free surface, the projectile is stopped by the resistance of the target metal to compression.

4. Liquid-Versus-Liquid Collisions

Liquid-versus-liquid collisions occur when liquid drops collide with a target liquid. Very little study has been made of collisions of this kind.

It was postulated by Opik [6] nearly twenty-five years ago, later by Pack and Evans [7], and recently by others [8] that at extremely high impingement velocities solid targets and projectiles will behave as though they were liquids. Opik stated, "The 'aerodynamic' pressure at the penetration of a meteor into rock is of the order of $10^7 - 10^8$ atmospheres, or more than 1,000 times the plastic limit of steel; no doubt all solid materials under such pressures must behave like liquids; thus the problem of meteor impact is the case of the impact of a liquid drop of given density δ into a liquid medium of density ρ ."

It has been found that, at sufficiently high impingement velocities, solid-sphere projectiles made of the soft ductile metals that are fired against targets of the same metal flow like liquids during and as a result of the collision. Pit depth for such solid-versus-solid collisions has been found [1] to be given by Eqs (1) and (2) that apply to collisions of liquid drops against metal plates.

If the impingement velocity is increased further, it is reasonable to suppose that the behavior predicted by Opik [6] will eventually be found; the target as well as the projectile will liquefy during the collision. For such collisions that occur at meteor velocities Opik [6] found that the impingement velocity has only a small effect upon the depth of penetration. If this is the case, the pit-depth-versus-velocity curve for such collisions should run almost parallel to the velocity axis. The penetration formula developed by Pack and Evans [7] has no velocity dependence.

It appears that the straight-line, low-velocity, liquid-versus-solid and solid-versus-solid pit-depth-versus-velocity curves for collisions of liquid drops and rigid steel spheres

with metal plates must approach the high-speed liquid-versus-liquid curve in some way when very high impingement velocities are reached. This is represented schematically in Figure 12 where dashed lines have been used to indicate projected types of behavior.

Equations (1), (2), (3), and (4) will not apply either in the transition regions or in the velocity range of high-speed liquid-versus-liquid collisions.

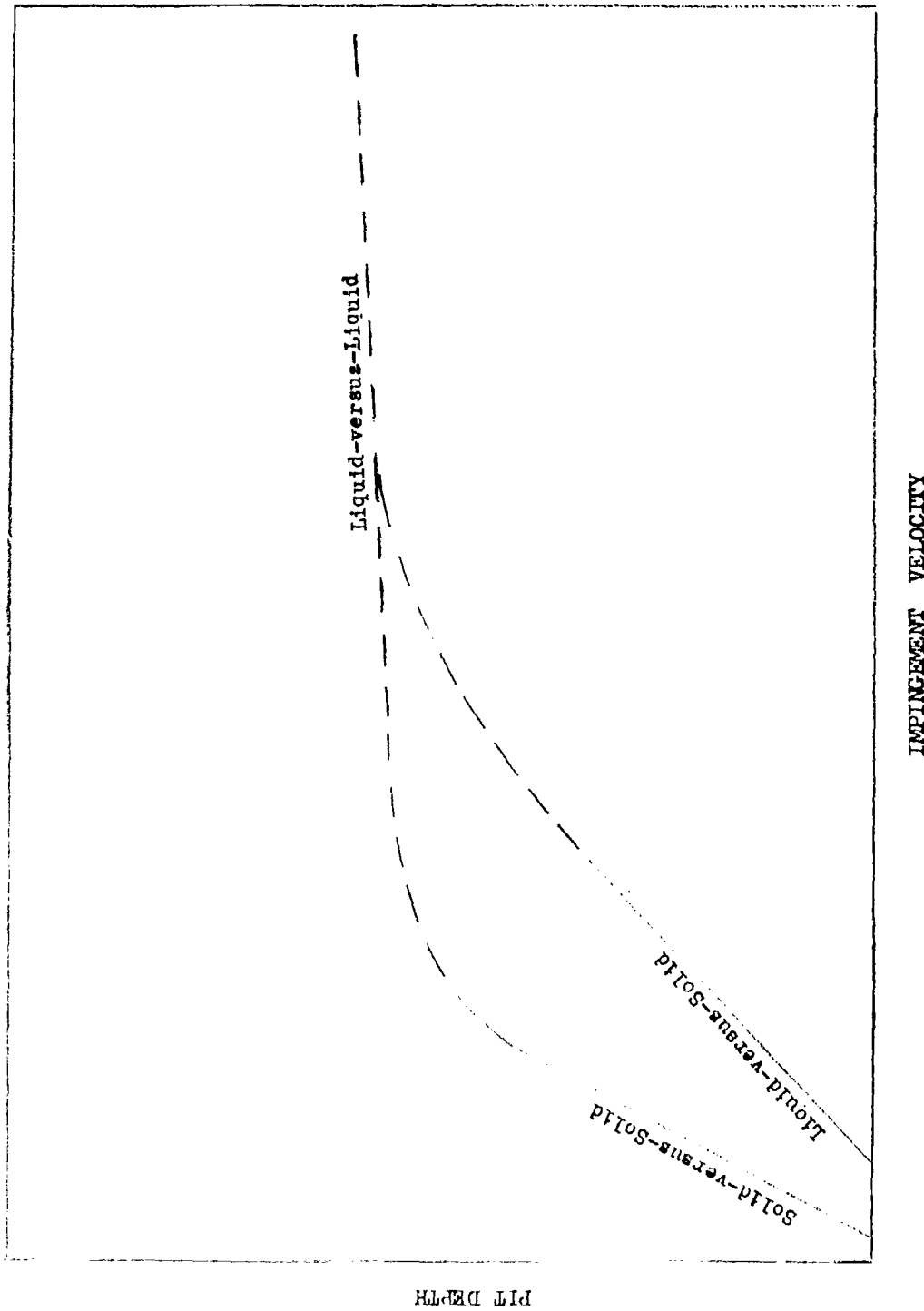


Figure 12. Schematic Representation of Projectile-Target Collision Types

REFERENCES

1. Olive Engel, Pits in Metals Caused by Collision with Liquid Drops and Soft Metal Spheres, NBS Journal of Research 62, 229 (1959)
2. A. C. Whiffin, The Use of Flat-ended Projectiles for Determining Dynamic Yield Stress, Proc. Roy. Soc. (London) 194A, 300 (1948)
3. L. Bergmann, Der Ultraschall, S. Hirzel Verlag, Stuttgart, 1954
4. A. C. Whiffin, communicated by letter
5. G. Thomas and J. Nutting, The Plastic Deformation of Aluminum and Aluminum Alloys, J. Inst. Metals 85, 1 (1956)
6. Ernst Opik, Researches on the Physical Theory of Meteor Phenomena I, Toimetused, Acta et Commentationes, Universitatis Tartuensis, XXX, A 4 (1936) (Tartu, Estonia)
7. D. C. Pack and W. M. Evans, Penetration of High-Velocity ('Munroe') Jets I and II, Proc. Phys. Soc. (London), LXIV B, 298 and 303 (1951)
8. See, for example, Proceedings of Third Symposium on Hypervelocity Impact, Vol. I, Armour Research Foundation of Illinois Institute of Technology, Chicago, Illinois, February, 1959

<p>UNCLASSIFIED</p> <p>NATIONAL BUREAU OF STANDARDS, Washington 25, D. C. PITS IN METALS CAUSED BY COLLISION WITH LIQUID DROPS AND RIGID STEEL SPHERES, by Olive G. Engel, June 1959. 41p. incl. illus. tables. (Project 7340) WADC TR 53-192, Part XIV (Contract No. AF 33(616)-59-12)</p> <p>Unclassified report</p> <p>A pit-depth-versus-velocity equation developed earlier for high-speed collision of liquid drops and soft, ductile metal spheres against targets of the soft and medium-hard metals was tested further with experimental data obtained using target plates of electrolytic tough pitch copper,</p>	<p>UNCLASSIFIED</p>
<p>UNCLASSIFIED</p> <p>(over)</p> <p>1100-O aluminum, and 2024-O aluminum. Projectiles used were mercury drops, water- drops, and steel spheres. It was found that numerical constants in the equation are different for projectiles that do not flow. Curves calculated by the equation were in agreement with the experimental data with the exception of steel-sphere impinge- ment against 2024-O aluminum. In this case work-hardening of the target metal may foster a mode of pit formation not con- sidered in the development of the equation.</p>	<p>UNCLASSIFIED</p>
<p>UNCLASSIFIED</p>	<p>UNCLASSIFIED</p>